A 17 month climatology of the cloud condensation nuclei number concentration at the high alpine site Jungfraujoch

Z. Jurányi,[1] M. Gysel,[1] E. Weingartner,[1] N. Bukowiecki,[1] L. Kammermann,[1] and U. Baltensperger[1]

Received 18 October 2010; revised 22 February 2011; accepted 9 March 2011; published 24 May 2011.

[1] Between May 2008 and September 2009 the cloud condensation nuclei (CCN) number concentration, N_{CCN}, was measured at the high alpine site Jungfraujoch, which is located in the free troposphere most of the time. Measurements at 10 different supersaturations (0.12%–1.18%) were made using a CCN counter (CCNC). The monthly median N_{CCN} values show a distinct seasonal variability with ~5–12 times higher values in summer than in winter. The major part of this variation can be explained by the seasonal amplitude of total aerosol number concentration (~4.5 times higher values in summer), but it is further amplified (factor of ~1.1–2.6) by a shift of the particle number size distribution toward slightly larger sizes in summer. In contrast to the extensive properties, the monthly median of the critical dry diameter, above which the aerosols activate as CCN, does not show a seasonal cycle (relative standard deviations of the monthly median critical dry diameters at the different supersaturations are 4–9%) or substantial variability (relative standard deviations of individual data points at the different supersaturations are less than 18–37%). The mean CCN-derived hygroscopicity of the aerosol corresponds to a value of the hygroscopicity parameter κ of 0.20 (assuming a surface tension of pure water) with moderate supersaturation dependence. N_{CCN} can be reliably predicted throughout the measurement period with knowledge of the above-mentioned averaged κ value and highly time-resolved (~5 min) particle number size distribution data. The predicted N_{CCN} was within 0.74 to 1.29 times the measured value during 80% of the time (94,499 data points in total at 10 different supersaturations).

Citation: Jurányi, Z., M. Gysel, E. Weingartner, N. Bukowiecki, L. Kammermann, and U. Baltensperger (2011), A 17 month climatology of the cloud condensation nuclei number concentration at the high alpine site Jungfraujoch, *J. Geophys. Res.*, *116*, D10204, doi:10.1029/2010JD015199.

1. Introduction

[2] Atmospheric clouds scatter and absorb short- and long-wave radiation; therefore they influence our climate. If their microphysical properties (e.g., droplet size, droplet density, cloud lifetime) change, their radiative properties will also change, thereby altering the magnitude of their climate impact [*Lohmann and Feichter*, 2005]. Since cloud droplets are formed by condensation of water on aerosol particles, those particles that are able to form a cloud droplet (commonly referred to as cloud condensation nuclei, CCN) play a key role in determining our climate [*Intergovernmental Panel on Climate Change* (*IPCC*), 2007] and precipitation [*Rosenfeld et al.*, 2008]. Our knowledge of aerosol-cloud interactions is incomplete and has the highest uncertainty among the anthropogenic radiative forcings [*IPCC*, 2007], and therefore understanding the factors influencing properties and abundance of atmospheric CCN is crucial. Part of this uncertainty can be attributed to the high temporal and spatial variability of the aerosol properties. This makes CCN measurements in various environments and during all seasons of the year essential.

[3] The CCN activation process of aerosol particles was studied many times on laboratory generated single component aerosols and mixtures [e.g., *Gerber et al.*, 1997; *Cruz and Pandis*, 1997; *Raymond and Pandis*, 2003; *Abbatt et al.*, 2005]. Numerous studies exist also on ambient aerosols [e.g., *Broekhuizen et al.*, 2006; *Dusek et al.*, 2006; *Chang et al.*, 2007; *Bougiatioti et al.*, 2009; *Lance et al.*, 2009; *Gunthe et al.*, 2009; *Kammermann et al.*, 2010a; *Rose et al.*, 2010] but these studies cover measurement periods of ~1 month and therefore are not able to elucidate the long-term seasonal variation of the CCN number concentration or properties. Long-term measurements [*Sihto et al.*, 2010] are rare, and comprehensive CCN climatology studies are still missing [*Medina et al.*, 2007].

[4] In this paper we present a long-term (17 months) study on the CCN number concentration at the high alpine site, Jungfraujoch (JFJ). The Jungfraujoch station is situated

[1]Laboratory of Atmospheric Chemistry, Paul Scherrer Institut, Villigen, Switzerland.

0148-0227/11/2010JD015199

in the Swiss Bernese Alps (46°33′N, 7°59′E) at 3580 m elevation on an anticline between the two mountains Jungfrau (4166 m asl) and Mönch (4107 m asl). The station's unique geographical situation offers the opportunity to measure continental background aerosols. Most of the time it stays in the free troposphere (FT) but sometimes it is also influenced by injections from the planetary boundary layer (PBL) [*Nyeki et al.*, 1998]. In summer, on average 20–40% of the air mass originates from the PBL whereas the same for winter is 5–10% [*Collaud Coen et al.*, 2011].

[5] Aerosol measurements at the JFJ have started more than 20 years ago [*Baltensperger et al.*, 1997], and this site has been part of the Global Atmosphere Watch (GAW) program of the World Meteorological Organization since 1995 [*Collaud Coen et al.*, 2007]. The following aerosol parameters are continuously monitored within the framework of GAW and EU programs (state in 2009): number concentration, number size distribution, scattering coefficient, absorption coefficient, PM1 (particulate matter with an aerodynamic particle diameter $D < 1$ μm) mass concentration, ionic composition in two size classes (PM1 and TSP, measured every 6th day for 24 h) and the CCN number concentration at 10 different supersaturations. The high altitude of the measurement site makes it possible to monitor the CCN number concentration in situ where cloud formation takes place [37% of the time the measurement site stays in clouds as shown by *Baltensperger et al.* [1998].

2. Experimental Setup

[6] All the instruments operated during the measurement period were connected to a heated total aerosol inlet, which allows all the aerosol particles and hydrometeors with $D <$ ~40 μm to enter. The inlet is heated to 25°C in order to evaporate any water, thereby releasing those particles that were activated as hydrometeors [*Weingartner et al.*, 1999; *Henning et al.*, 2002]. Thus the sampled aerosol consists of all particles, i.e., interstitial particles as well as residuals of cloud droplets and ice crystals. The instruments were operated at a laboratory temperature of ~25°C. Heating the particles from ambient temperatures to 25°C might also cause evaporation of other semivolatile aerosol components. *Nessler et al.* [2003] showed by measuring the number size distribution simultaneously at ambient and room temperature at JFJ that evaporation effects occur for a fraction of the particles with $D <$ ~100 nm, while differences at D > ~100 nm could largely be explained by evaporation of water.

[7] A Continuous-Flow Streamwise Thermal-Gradient CCN Chamber (CCNC, Droplet Measurement Technologies, model CCN-100;) [*Roberts and Nenes*, 2005] was directly connected to the total inlet (total flow rate of 1 L min^{-1}, 10:1 sheath-to-sample flow ratio) in order to measure the total polydisperse CCN number concentration (N_{CCN}) as a function of time and at different supersaturations (*SS*). The *SS* in the CCNC is determined by the applied temperature gradient in the activation column's wetted wall. Every measurement cycle consisted of applying 10 different temperature gradients in the CCNC (ΔT = 2–15°C, *SS* = 0.12–1.18%) and lasted ~60 minutes, including the time which was needed to allow for stabilization of the *SS*. The CCN active particles (i.e., those having a lower critical *SS* than the *SS* applied in the CCNC) will grow into the supermicron size range while they pass the activation column and will afterward be counted as CCN by an optical particle sizer. Nonactivated particles remain well below the lower threshold diameter (typically set to 1 μm) and are not counted as CCN.

[8] The calibration of the CCNC was verified once every month on average by using nebulized, dried, and size selected ammonium sulfate particles, following the procedures described by *Rose et al.* [2008]. At a certain temperature gradient the critical dry diameter, $D_{0,crit}$, where 50% of the singly charged ammonium sulfate particles were activated, was determined by fitting the sum of two sigmoid functions to the activation curve. The critical *SS* corresponding to the measured $D_{0,crit}$ was obtained from the ADDEM model [*Topping et al.*, 2005]. During calibrations, 10 different temperature gradients were set in the CCNC such that the resulting *SS* values covered the range from 0.07 to 1.1% *SS*, similar to the *SS* range of the measurement. During the 17 month measurement campaign the calibration curve ($SS = -0.139\% + 0.097\frac{\%}{K} \cdot \Delta T$) remained stable. The *SS* values obtained at any temperature gradient and during all calibration measurements deviated maximally ±8% from the *SS* values calculated according to the above calibration curve. Therefore we attribute an uncertainty of ±8% to the reported *SS* values.

[9] The aerosol number size distribution was monitored for diameters between 16 and 570 nm with a scanning mobility particle sizer (SMPS). It consisted of a differential mobility analyzer (DMA, TSI 3071) and a condensation particle counter (CPC, TSI CPC 3775; during a brief period a TSI CPC 3772). The size distribution was measured every 6 min, with an up scan time of 300 s. The DMA was operated with 0.3 L min^{-1} sample air flow rate and a closed-loop excess and sheath air setup with a flow rate of 3 L min^{-1} (1 L min^{-1} sample flow rate and 5 L min^{-1} excess sheath air flow rate during the brief period when the CPC model 3772 was used). The sheath flow rate was continuously regulated by a mass flow controller, whereas pressure and temperature measurements were used to calculate the mass flow set point such that the volumetric flow remained constant. All flow rates were verified monthly with a bubble flowmeter. Sizing accuracy was checked with certified polystyrene latex (PSL) spheres of different diameters. The measured size agreed within ±3% with the nominal size of the PSL spheres.

[10] During the measurement period the total number concentration of particles with diameter >10 nm (N_{10}) was monitored by a CPC (TSI CPC 3010 until 25 June 2008, TSI CPC 3772 from then onward). The CPC data was used to validate and correct the SMPS data by comparing N_{10} with the total particle number concentration (N_{16-570}) obtained by integrating the number size distribution, following the approach of *Jurányi et al.* [2010]. According to this comparison the SMPS data were corrected by a size-independent, time-dependent factor between 0.7 and 1.3 (see Appendix A for more details).

[11] Between May 2008 and May 2009 a custom-built hygroscopicity tandem differential mobility analyzer (HTDMA) was deployed to determine the hygroscopic properties of the particles at subsaturated relative humidity (RH). Hygroscopic diameter growth factors (*GF*) at a constant RH of 90% were measured for six different dry dia-

meters (D_0 = 35 nm, 50 nm, 75 nm, 110 nm, 165 nm, 265 nm). Technical details of the HTDMA and main results of these measurements are reported by *Kammermann et al.* [2010a].

3. Theory and Data Analysis

3.1. Calculation of the Hygroscopicity Parameter κ

[12] The equilibrium vapor pressure over a curved surface of a solution is described by the Köhler equation [*Köhler*, 1936; *McFiggans et al.*, 2006]. Aerosol hygroscopic properties below and above water vapor saturation, i.e., diameter growth factors and critical diameters for CCN activation, respectively, can be linked using the Köhler equation and an appropriate parametrization of the water activity. We used the κ single-parameter water activity parametrization from *Petters and Kreidenweis* [2007]. The semiempirical κ parameter takes values between 0 (nonhygroscopic but wettable) and ~1.3 (most hygroscopic salts) for atmospheric aerosols.

[13] HTDMA derived κ values can be directly obtained by inserting the measured GFs into the Köhler equation [*Petters and Kreidenweis*, 2007]. Determining CCNC derived κ values needs an iterative approach: $D_{0,\mathrm{crit}}$, derived from N_{CCN} and number size distribution data, is first set into the Köhler equation, and then κ has to be varied until the corresponding critical *SS* equals the *SS* value at which N_{CCN} was measured. The surface tension of the solution droplet is also a key parameter in the Köhler equation. We used the surface tension of pure water in all our calculations. This is a common assumption since we deal with dilute solutions at the point of activation, and the CCN closure study conducted at the JFJ by *Jurányi et al.* [2010] indicated that the surface tension of water can indeed be used for calculations at the point of activation.

3.2. Calculation of the Critical Diameter for CCN Activation

[14] The critical diameter for CCN activation is well defined in the case of a perfectly internally mixed aerosol; that is, all particles with diameter $>D_{0,\mathrm{crit}}$ will act as CCN at a given *SS*, while all particles with diameter $<D_{0,\mathrm{crit}}$ will remain in the interstitial phase. Atmospheric aerosols are typically not perfectly internally mixed and with that the transition between 0% and 100% activated fraction occurs over a range of diameters. Such a $D_{0,\mathrm{crit}}$ distribution can only be derived from size-resolved CCN measurements [*Su et al.*, 2010]. In this study we have only particle number size distribution and polydisperse CCN number concentration measurements available. Nevertheless, an effective $D_{0,\mathrm{crit}}$ can be obtained for each supersaturation set in the CCNC (SS_{set}) with assuming a sharp activation cutoff leading to the following well-established implicit equation:

$$N_{\mathrm{CCN}}(SS_{\mathrm{set}}) = -\int_{D_{\max}}^{D_{0,\mathrm{crit}}(SS_{\mathrm{set}})} \frac{dN}{d\log D}(D)\, d\log D. \qquad (1)$$

[15] The number size distribution is integrated starting from its upper end. The diameter at which the integrated number concentration equals the measured $N_{\mathrm{CCN}}(SS_{\mathrm{set}})$ corresponds then to $D_{0,\mathrm{crit}}(SS_{\mathrm{set}})$. Assuming a sharp activation cutoff is a valid and useful approach when it comes to calculating N_{CCN} from particle number size distribution data for several reasons: First, treating an externally mixed aerosol as internally mixed hardly changes the calculated N_{CCN} for not freshly emitted aerosols [e.g., *Rose et al.*, 2010; *Kammermann et al.*, 2010b; *Wang et al.*, 2010]. Second, the aged aerosol encountered at the remote JFJ site is anyway largely internally mixed most of the time [*Sjogren et al.*, 2008; *Kammermann et al.*, 2010a]. Third, using the effective $D_{0,\mathrm{crit}}$ obtained from equation (1) together with size distribution data at the time when $D_{0,\mathrm{crit}}$ was determined for calculating N_{CCN} provides by definition the correct value. Uncertainties in calculated N_{CCN} arising from applying $D_{0,\mathrm{crit}}$ to size distribution data measured at other times are dominated by the temporal variability of $D_{0,\mathrm{crit}}$ rather than mixing state effects.

3.3. Alpine Weather Statistic

[16] We used the Alpine Weather Statistic (AWS) [*Schüepp*, 1979] synoptic weather classification system in order to investigate the PBL influence on N_{CCN}. This classification is based on the daily analysis of the pressure distribution at the surface and at the 500 hPa level. The classification considers a circular area centered ~80 km east of JFJ with a radius of 222 km, covering the Swiss Alps and parts of Austria, Italy and France. The 40 subcategories were clustered into 5 main synoptic weather classes, following the examples of *Kammermann et al.* [2010a] and *Collaud Coen et al.* [2011]. For the advective class (Ax), horizontal motion of the atmosphere is dominant. This results in horizontal wind over a flatter rain. However, the geography of the Alps might transform part of this horizontal motion into vertical motion. The second main class is the convective class, where the vertical motion of the atmosphere is dominant. The convective class is divided into 3 subclasses according to the direction of the vertical motion: convective cyclonic (CC), convective anticyclonic (CA) and convective indifferent (CI). The CC weather type is associated with lifting synoptic motion, CA with subsidence and CI with small-scale circulations. The ascent of air for the CC type results in adiabatic cooling and cloud formation with subsequent precipitation, whereas the large-scale subsidence for CA type results in clear and sunny weather, where injections of PBL air into the FT frequently occur. If both horizontal and vertical motion is present we talk about a mixed synoptic weather type (M).

4. Results and Discussion

[17] The 17 month measurement period took place between May 2008 and September 2009. During this period the CCN number concentration at 10 different *SS* (0.12–1.18%) was measured with a time resolution of ~1h. The fractional data coverage of the CCN measurement during the 17 month period varied between 47% and 100% on a monthly basis with an average value of 83% (Table 1, F_{meas} column). Gaps in the data set are caused by calibration measurements and instrumental problems. Different aspects of the CCN properties observed during this period are discussed in the following.

Table 1. The Annual and Monthly Median Values of N_{CCN} at All Investigated Supersaturations and of the Integrated Number Size Distribution ($N_{16–570}$)[a]

SS	0.12%	0.24%	0.35%	0.47%	0.59%	0.71%	0.83%	0.95%	1.07%	1.18%	$N_{16–570}$	F_{meas}
Annual	43.4	94.7	128.8	150.8	168.8	183.8	199.7	214.5	226.7	257.1	320.4	0.83
						2008						
May	90.4	158.9	210.1	246.8	277.4	313.8	349.2	376.7	387	434	542.8	0.80
June	89.5	172.2	231.2	270.6	305.4	336.7	379.6	388.3	389.1	441	488.5	0.97
July	109.4	224.1	289.6	340.4	387.3	433.9	474.2	499.6	497	563	655.1	0.75
August	76.6	186.6	269.6	319.7	354.7	394.9	445.1	471.1	468.7	524.2	578.8	0.99
September	77.9	141.8	181.7	207.5	230.1	250.3	276.7	283.6	289	323.1	418.2	0.92
October	47.5	100.5	130	148.6	164.7	173.2	186.1	195.6	201.2	222.7	286.5	0.77
November	16.9	42.4	57.9	69.0	78.6	86.9	95.9	102.5	109	131.8	215	0.71
December	16.66	39.5	51.3	60.9	67.8	74.3	81.9	88.3	93.7	113.4	155.7	0.79
						2009						
January	11.4	27.8	37.1	45.0	52.8	60.7	69.8	79.3	86.6	113.6	194.6	0.88
February	18.5	41.3	54.4	61.7	70.0	79.1	87.8	97.7	105.9	125.0	190.9	1
March	32.1	75.6	103.2	121.0	134.4	143.4	158.7	173.3	178.7	208.3	261.5	0.82
April	124.8	214.7	267.3	294.4	322.4	350.7	387.9	412.6	421.4	480.8	514.8	0.90
May	116.1	196.0	260.8	295.2	325.1	382.1	416.5	439.5	460.3	513.4	688.0	0.53
June	73.9	156.3	209.2	231.7	256.5	280.4	307.5	331.0	342.8	379.2	565.8	0.75
July	118.2	239.1	303.7	344.0	377.2	427.8	448.9	475.2	473.5	529.7	635.4	0.47
August	143.2	259.2	324.9	365.3	396.6	447.9	463.8	485.3	485.0	535.4	608.3	1
September	87.1	161.0	201.0	226.4	244.2	257.8	281.8	293.4	302.5	339.8	386.0	1

[a]The annual median values are determined using data from May 2008 to April 2009 only, in order to prevent overrepresentation of the warmer months. All concentrations are given in cm^{-3}. The F_{meas} column contains the fractional data coverage of N_{CCN} during the measurement period.

4.1. Diurnal Variation of CCN Properties

[18] During colder periods the JFJ stays in the free troposphere whereas during warmer periods JFJ is influenced by injections from the PBL. Air parcels below the site are heated up during the day and reach the altitude of the measurement site by thermal convection [*Nyeki et al.*, 2000]. On those days when injections from the PBL reach the JFJ, a diurnal cycle is present in all measured extensive aerosol properties [*Lugauer et al.*, 1998; *Collaud Coen et al.*, 2007; *Kammermann et al.*, 2010a; *Collaud Coen et al.*, 2011] such as, e.g., number concentration, mass concentration, light scattering coefficient or light absorption coefficient. In winter, days with a diurnal cycle are rarely present, as the thermal convection is not strong enough to transport air masses from the PBL up to the JFJ. Here we investigate the diurnal patterns of CCN properties in order to determine the effect of PBL influence.

[19] The diurnal pattern of N_{CCN} was determined for each season separately due to the pronounced seasonality of the PBL influence (note that because of the total duration of 17 months, some months are twice and some only once represented in the averages). Figures 1a–1d show the mean diurnal patterns of N_{CCN} for all four seasons and all investigated *SS*.

[20] A pronounced diurnal pattern of N_{CCN} is observed in spring, summer and autumn. The maximum N_{CCN} is reached at ~1500–1900 (local winter time, UTC + 1) and the minimum at ~0300–0900 UTC + 1. The latter agrees well with the time when *Nyeki et al.* [1998] observed minimum concentrations of other extensive aerosol parameters and can therefore be defined as the time of day when the measurement site generally stays in the free troposphere. Therefore filtering all data according to this time window can be used to investigate the CCN properties in the free troposphere even though we do not cover all periods when the site is in the FT. In the following, FT conditions refer to the subset of data measured between 0300 and 0900 UTC + 1. In spring, summer and autumn the factor between maximum and minimum N_{CCN} of the mean diurnal pattern is roughly 1.5 and relatively constant across all *SS*. In winter the diurnal pattern almost disappears with an amplitude of only a factor of 1.2 and much shorter time of enhanced N_{CCN}. This confirms that in winter the site is almost always in the undisturbed free troposphere during the whole day.

[21] For the summer season the mean diurnal pattern of $D_{0,crit}$, determined from N_{CCN} and number size distribution data according to equation (1), is shown in Figure 2, in order to investigate potential differences between the hygroscopicity of the free tropospheric and the PBL influenced aerosol. A weak diurnal pattern can be identified, with slightly increased $D_{0,crit}$ values during the afternoon when the PBL influence is present, indicating that these particles are slightly less hygroscopic than the background FT aerosol. The maximum and minimum $D_{0,crit}$ observed in summer at 0200–0700 UTC + 1 and 1000–1900 UTC + 1, respectively, translate into median κ values (including data from all *SS*) of ~0.24 and ~0.17. A similar diurnal pattern of $D_{0,crit}$ can be identified in autumn, while in spring no significant increase of $D_{0,crit}$ during the afternoon can be seen (not shown). *Kammermann et al.* [2010a] also reported a similar diurnal pattern with slightly decreasing particle hygroscopicity during PBL influence based on HTDMA measurements of hygroscopic diameter growth factors measured at 90% RH. The increase of $D_{0,crit}$ under PBL influence dampens the diurnal pattern of N_{CCN} slightly but the fact that the latter is still clearly observed shows that the distinct increase in the particle number concentration has the dominant influence.

[22] The influence of the PBL on the diurnal pattern of N_{CCN} was further investigated by splitting the summer data–when PBL influence is most prominent–according to the

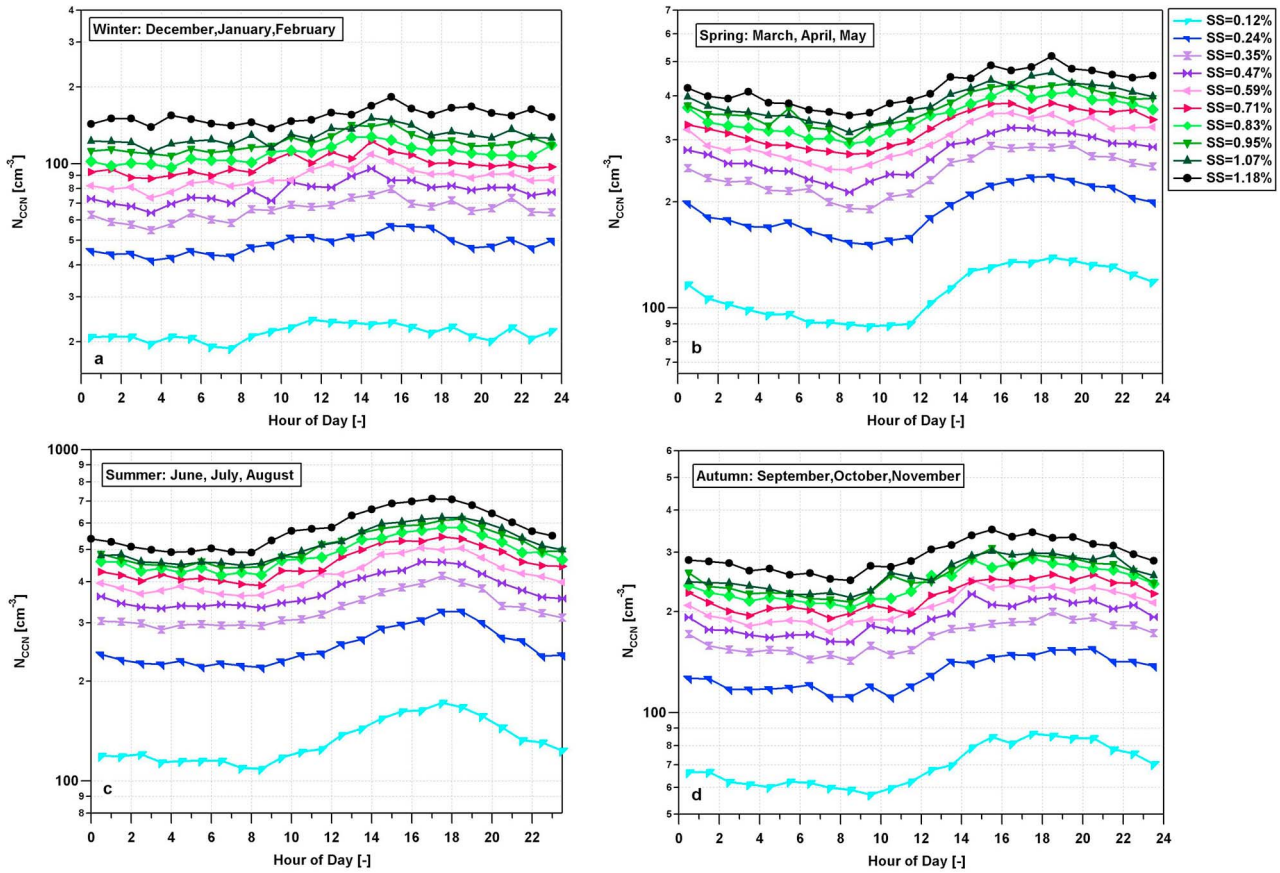

Figure 1. Mean diurnal pattern (local winter time, UTC+1) of N_{CCN} in the different seasons.

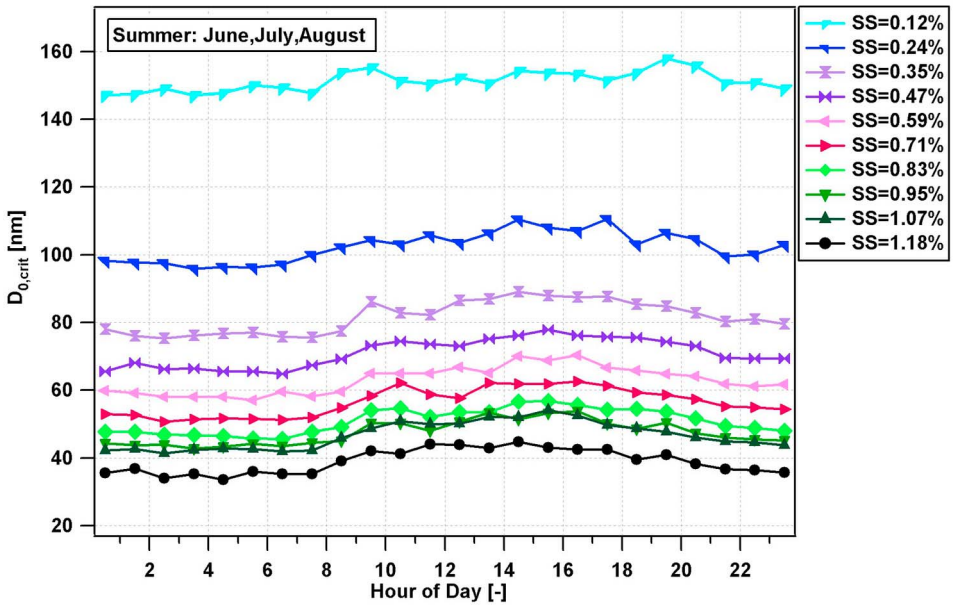

Figure 2. Diurnal pattern (local winter time, UTC+1) of the critical dry diameter for CCN activation ($D_{0,crit}$) in summer, when PBL influence is frequently observed in the afternoon.

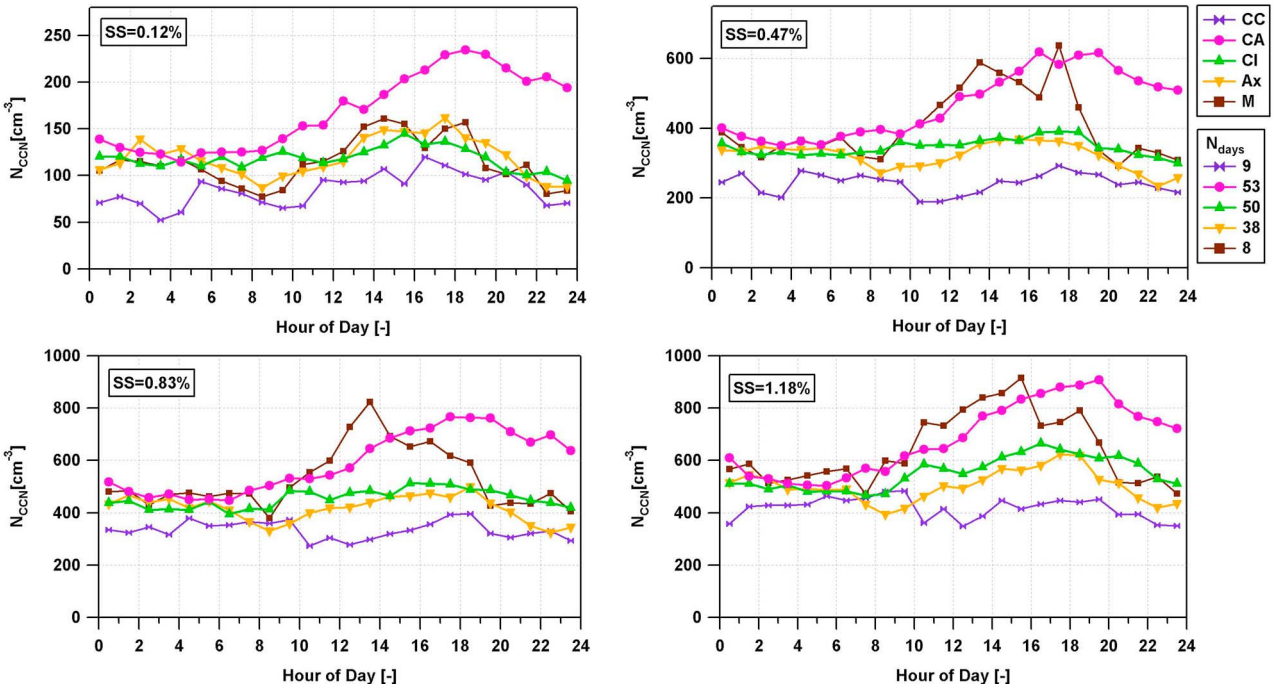

Figure 3. Diurnal pattern (local winter time, UTC+1) of N_{CCN} in summer for the different synoptic weather types (Ax, advective; CC, convective cyclonic; CI, convective indifferent; CA, convective anticyclonic; M, mixed). N_{days} is the number of days when the particular synoptic weather type was present.

synoptic weather types from the AWS (see section 3.3). Data for the M and CC classes have to be treated with caution as less than 10 days are included in the average. The diurnal patterns for the different synoptic weather classes are shown in Figure 3 for four example *SS*. As expected, the observed diurnal patterns agree qualitatively across all *SS*. The CA class exhibits the most pronounced diurnal cycle, if we exclude the M class. This is in agreement with the findings of *Collaud Coen et al.* [2011], who reported the strongest PBL influence at the JFJ for the CA class with, about 40% of the air mass originating from the PBL under these extreme conditions. For this class the amplitude of the mean diurnal cycle of N_{CCN} is roughly a factor of 2 across all *SS*. The daily minimum N_{CCN} values occur between ~0300 and 0900 UTC+1, and they are largely independent of the synoptic weather type. This confirms that PBL influence in this time window is negligible and that this time window can be used to investigate FT conditions without further filtering. It is not worth speculating about the reasons for the slightly lower minimum values of N_{CCN} during CC days as statistics are very limited.

4.2. Seasonality of the CCN Number Concentration and the Activated Fraction

[23] *Reutter et al.* [2009] used a cloud parcel model to show that the cloud droplet number concentration becomes proportional to the particle number concentration in the aerosol-limited regime at high ratios of updraft velocity to particle number concentration and practically independent of the updraft velocity. The CCN number concentrations observed at the JFJ are very low even at the highest *SS* (monthly median values between 113 cm^{-3} and 563 cm^{-3}; see Table 1), such that cloud droplet activation is likely to occur in the aerosol-limited regime most of the time. An anthropogenic increase of particle number concentration can thus be expected to influence cloud properties.

[24] The analysis of diurnal patterns in section 4.1 revealed a strong seasonal cycle of the influence from injections of more polluted PBL air. As a consequence also N_{CCN} shows a strong seasonal cycle with much higher values during the warmer seasons, similar to all other extensive aerosol properties. A detailed analysis of monthly distributions of N_{CCN} (10th, 25th, 50th = median, 75th and 90th percentiles) is presented in Figure 4 for four different example *SS* as well as in Table 1 for all *SS* (median values only). Note that the annual median values shown in Table 1 are determined using data from May 2008 to April 2009 only, in order to prevent overrepresentation of the warmer months.

[25] The annual median values of N_{CCN} naturally decrease with decreasing SS and there is a factor of 6 difference between the highest (*SS* = 1.18%) and the lowest (*SS* = 0.12%) supersaturation (N_{CCN} = 257 and 43 cm^{-3} at *SS* = 1.18% and 0.12%, respectively). However, the seasonal cycle of N_{CCN} is of similar magnitude such that N_{CCN} = 124 cm^{-3} at *SS* = 0.12% in summer is comparable to N_{CCN} = 113 cm^{-3} at *SS* = 1.18% in winter. The amplitude of the seasonal cycle is a factor of ~12 at the lowest *SS* (Figure 4a) and decreases to a factor of ~5 at the highest *SS* (Figure 4d). At the same time the amplitude is only a factor of ~4.4 for N_{16-570} (F_{meas} column of Table 1),while the pattern is qualitatively similar. This means that the seasonal cycle of total particle number concentrations explains the seasonal cycle of N_{CCN} for the most part, but not completely.

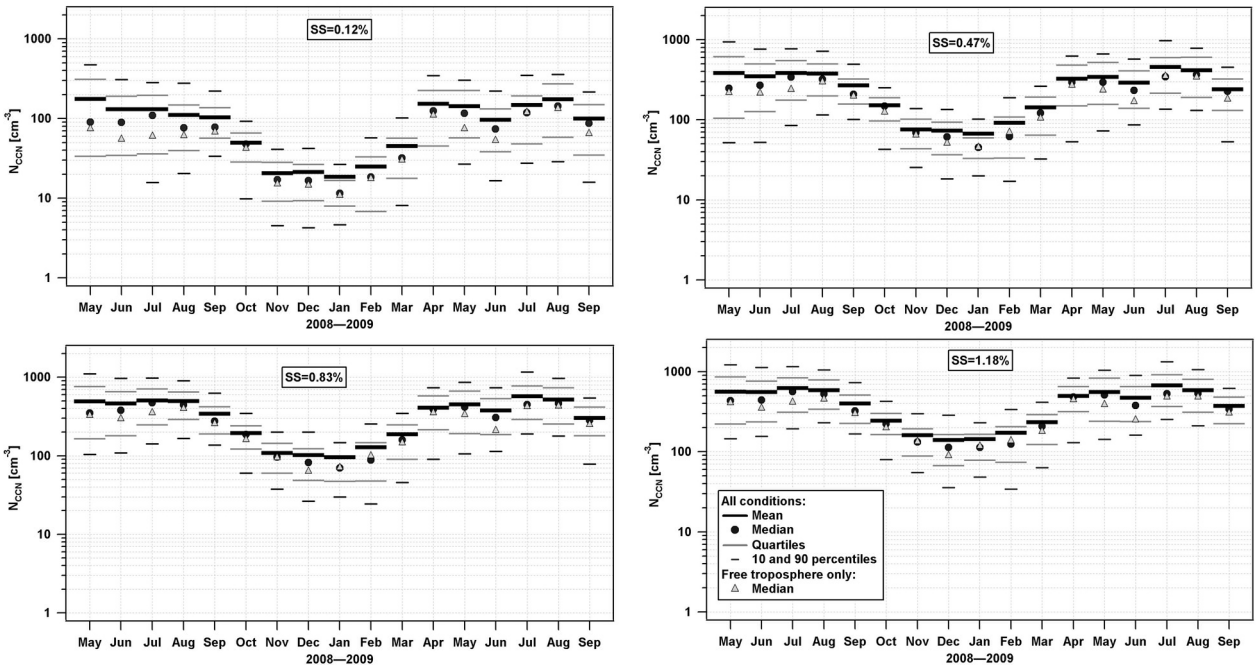

Figure 4. Seasonal pattern of the monthly distribution of the CCN number concentration at four example supersaturations (0.12%, 0.47%, 0.83%, and 1.18%) for all conditions and of the median value for FT conditions only (0300–0900 UTC+1).

[26] A separate analysis of the seasonal pattern of N_{CCN} during the time window 0300–0900 UTC + 1, when the site is almost exclusively in the lower FT throughout the whole year is also presented in Figure 4. N_{CCN} during FT conditions also exhibits a distinct seasonal cycle, with an amplitude of a factor of ~11.6–4.7 (at SS = 0.12–1.18%), which is only slightly smaller compared to all conditions. This is very likely due to residual layers in the FT that carry history from the PBL. In winter virtually no difference is observed between N_{CCN} during FT and all conditions, as PBL influence is virtually absent (see also Figure 1). In summer, when PBL influence is most prominent, N_{CCN} during all conditions are generally somewhat higher compared to FT conditions. However, depending on synoptic weather conditions PBL influence can also be negligible during prolonged periods in summer, as for example in July 2009, when N_{CCN} were found to be virtually equal for FT and all conditions. With the above facts we can state that PBL influence during the warmer season only causes a small enhancement of the seasonal amplitude of N_{CCN} during all conditions compared to FT conditions.

[27] Monthly statistics of the activated fraction (AF), i.e., CCN number concentration divided by the integrated CN number concentration, (AF = N_{CCN}/N_{16-570}), are shown in Figure 5 for four example SS. At the highest investigated SS (1.18%) the dominant fraction of the aerosol is CCN active (AF = 60–92%), in contrast to the lowest SS (0.12%), where the monthly median AF is as low as 6–25%. The AF exhibits a consistent seasonal pattern across all SS with highest values in summer and lowest values in winter. The amplitude of the difference between summer and winter decreases from a factor of ~4 at SS = 0.12% to a factor of ~1.5 at SS = 1.18%. The seasonal cycle of AF amplifies the seasonal cycle of N_{CCN}. Its contribution is roughly similar to the contribution from the seasonal cycle of the total particle number concentration at the lowest SS, while it becomes less important with increasing SS. Based on this analysis, we can conclude that changes of both extensive (total particle number concentration) and intensive aerosol properties (activated fraction) contribute significantly to the seasonal cycle of N_{CCN}. For FT conditions only, both the amplitude of the seasonal cycle and the actual absolute values of AF are very similar to those from all conditions (not shown here).

[28] The seasonal cycle of the AF can have two different causes: either the particle hygroscopicity and with that the critical dry diameter for CCN activation varies and/or the shape of the particle number size distribution varies such that the number fraction of particles above the activation cutoff changes systematically with season. The influence from these effects is addressed in section 4.3.

4.3. Critical Diameter for CCN Activation

[29] The effective critical dry diameter ($D_{0,crit}$) for CCN activation was calculated according to equation (1) as a function of time and SS from the N_{CCN} and particle number size distribution data as detailed in section 3.2. The quartile diameters of the monthly distributions of $D_{0,crit}$ along with the annual median values (blue lines) are presented in Figure 6. Only four example SS (0.12%, 0.47%, 0.83%, 1.18%) are shown for simplicity as the key feature is similar for all investigated SS: $D_{0,crit}$ is essentially independent of the season. This is in agreement with the observation from *Kammermann et al.* [2010a], who found that hygroscopic diameter growth factors at 90% RH are also largely independent of the season at the JFJ. Contrary to this, a signif-

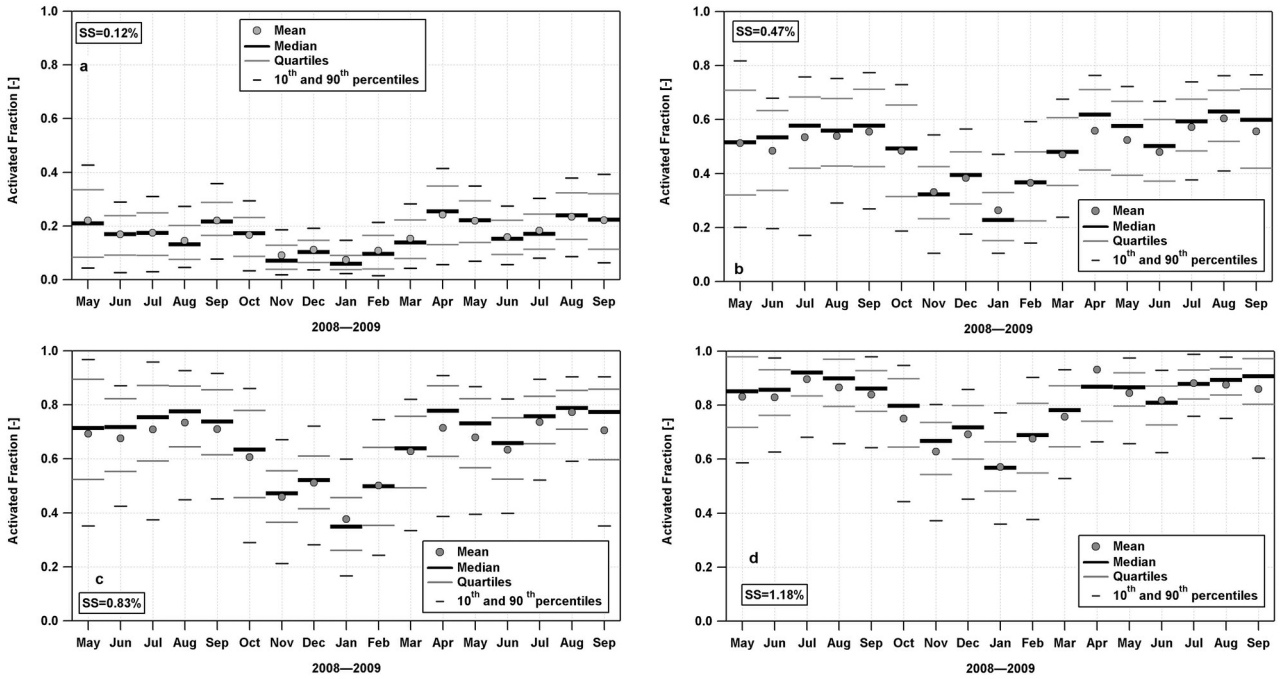

Figure 5. Seasonal pattern of the monthly distribution the activated fraction (AF; see text for definition) at four example supersaturations (0.12%, 0.47%, 0.83%, and 1.18%).

icant seasonal pattern of the diameter deciles of the normalized, monthly averaged number size distribution was observed (Figure 6, gray lines). The median particle diameter varies for example between ~40 nm in winter and ~80 nm in summer.

[30] Comparison of $D_{0,crit}$ with the diameter deciles in Figure 6 allows determining the monthly AF directly: for example, in December 2008 at $SS = 0.83\%$ the $D_{0,crit}$ value lies on the 5th decile line of the number size distribution. This means that on average 50% of the particles are larger than $D_{0,crit}$, and therefore AF = 0.5. A quantitative assessment of the relative importance of aerosol hygroscopicity and shape of the number size distribution for the seasonal pattern of N_{CCN} is possible by comparing the seasonal patterns of $D_{0,crit}$ (aerosol hygroscopicity) with the seasonal patterns of the diameter deciles of the number size distribution. At almost any *SS* the difference between the highest and lowest monthly median $D_{0,crit}$ is smaller than the difference between two neighboring diameter deciles of the number size distribution. In contrast, lines of constant diameter cross 2–4 different diameter deciles in the course of a season. This means that the seasonal variation of the aerosol hygroscopicity causes at most a change of 0.1 in the value of the AF, whereas the variations of the size distribution cause changes up to 0.4. In summary we can state that variations of the size distribution's shape dominate the seasonal pattern of AF at the JFJ; that is, variability of size matters much more than variability of hygroscopicity (composition, following *Dusek et al.* [2006]).

[31] The $D_{0,crit}$ values do not show high variability within 1 month either. This is reflected in the small difference between the median and the lower or upper quartiles, which is on average as small as 5–8 nm for all *SS* (whiskers in Figure 6). Consequently the CCN activation behavior at the JFJ and for the free troposphere can be very well described by a single time-independent $D_{0,crit}$ value for a given *SS*, which ranges from 147 nm at $SS = 0.12\%$) to 36 nm at $SS = 1.18$ (see Table 2 for annual median values of $D_{0,crit}$ for all investigated *SS*).

[32] The $D_{0,crit}$ values from the different *SS* are further converted into the commonly used hygroscopicity parameter κ (see section 3.1) and are listed in Table 2. The κ values can be directly compared in between different *SS* and with literature data from other CCN or hygroscopic diameter growth factor measurements. Box plots of the κ distributions at four example *SS* are shown in Figure 7 for all data as well as for the subset FT conditions. In section 4.1 we have shown that a strong PBL influence causes a slight reduction in the particle hygroscopicity. However, this effect largely disappears in the annual data, which is reflected in the fact that differences between all data and FT conditions are virtually nonexistent. This confirms the result by *Kammermann et al.* [2010a] that the PBL has a negligible effect on particle hygroscopicity in the annual average.

[33] Figure 7 also reveals an increasing variability of κ with increasing *SS* (corresponding to decreasing $D_{0,crit}$). This is not unexpected and in agreement with literature [*Swietlicki et al.*, 2008], given that smaller particles tend to be more heterogeneous than larger particles as they have typically been formed or emitted more recently and thus may have a different chemical composition. Furthermore, κ values increase with increasing particle diameter except at the smallest particle diameter (highest *SS*) as can be seen from the annual median values listed in Table 2 (the monthly κ distributions at 4 example *SS* are shown in Figure 8). Median κ values of individual *SS* range between 0.13 at

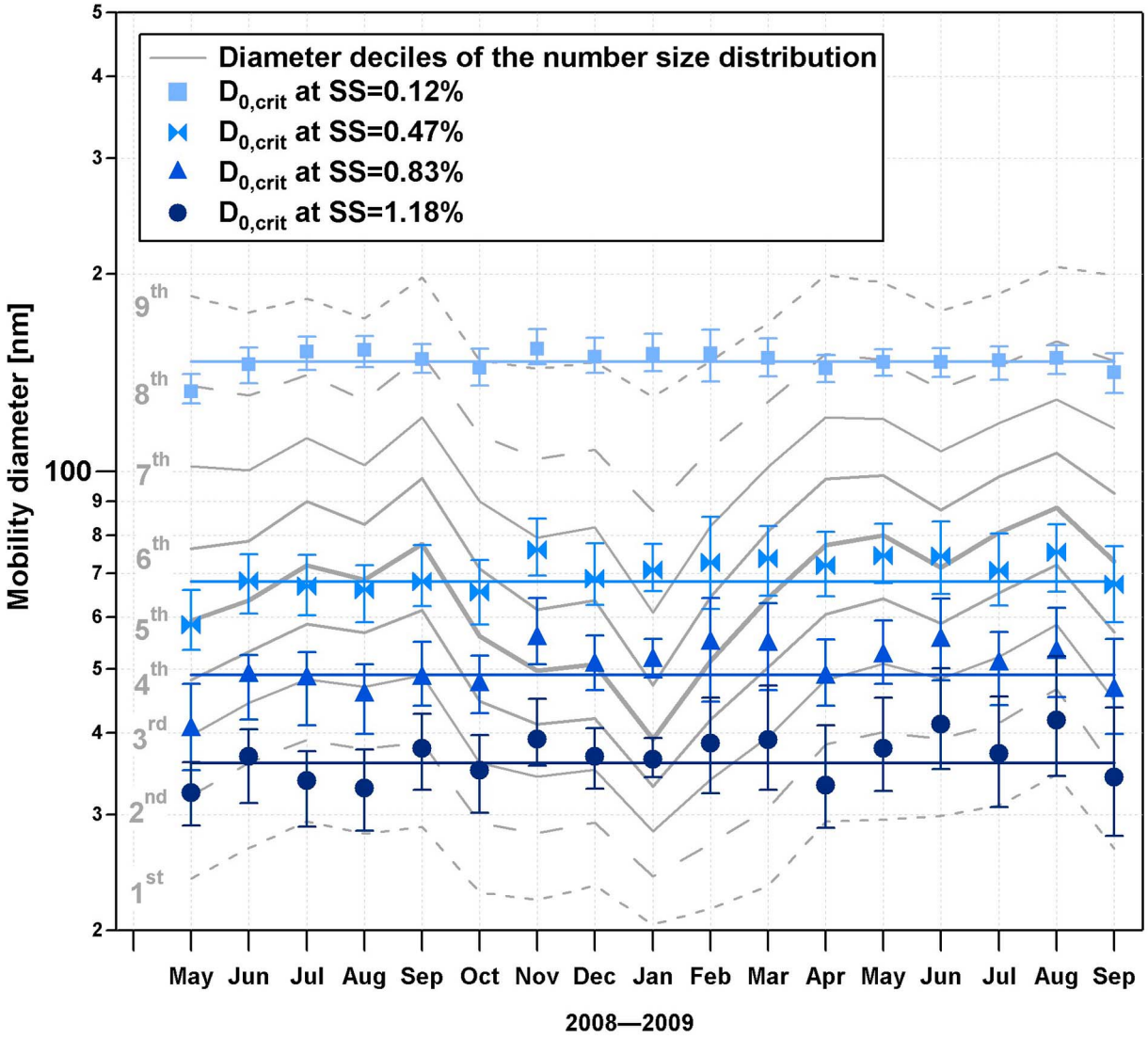

Figure 6. Monthly median values of the critical dry diameter ($D_{0,crit}$) for CCN activation at different supersaturations (blue symbols; the whiskers are drawn to the lower and upper quartiles). The diameter deciles of the normalized, monthly averaged number size distribution are shown as gray lines.

high *SS* and 0.29 at low *SS*, and the overall median CCN-derived κ value is 0.20. This value is within the range of the global mean κ values for continental regions (0.27 ± 0.21), whereas the mean value for marine regions (0.72 ± 0.24) is much higher [*Andreae and Rosenfeld*, 2008; *Pringle et al.*, 2010]. Above we have shown that $D_{0,crit}$ does not have a clear seasonal pattern (Figure 6) and therefore κ does not have one either (Figure 8). The month-to-month variations of $D_{0,crit}$ and κ are by definition anticorrelated.

4.4. Closure Between Subsaturated and Supersaturated RH Conditions

[34] This study provides a complete year of parallel measurements of hygroscopic diameter growth factors at RH = 90% (HTDMA), polydisperse CCN number concentrations (CCNC) and particle number size distribution (SMPS). This gives us a unique chance for a long-term

Table 2. The 25th Percentile, Median, and 75th Percentile Values of the Critical Dry Diameter ($D_{0,crit}$) and κ Parameter for the Measurement Period at the Different Supersaturations

	$D_{0,crit}$ (nm)			κ		
SS (%)	25th	50th	75th	25th	50th	75th
0.12	138	147	157	0.24	0.29	0.35
0.24	91	100	109	0.18	0.23	0.30
0.35	71	79	88	0.15	0.21	0.29
0.47	61	68	77	0.12	0.17	0.25
0.59	54	61	69	0.11	0.16	0.23
0.71	48	54	61	0.1	0.15	0.22
0.83	43	49	56	0.1	0.15	0.23
0.95	41	46	52	0.09	0.14	0.21
1.07	38	44	49	0.08	0.13	0.20
1.18	31	36	41	0.12	0.19	0.30

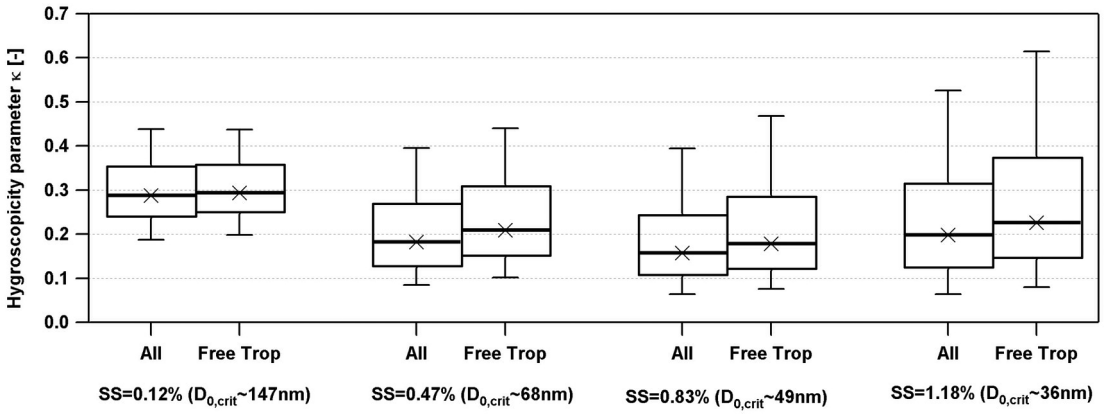

Figure 7. The 10th, 25th, 50th (median), 75th, and 90th percentiles of the κ distributions for all data and for the subset free tropospheric condition at four different example supersaturations (0.12%, 0.47%, 0.83%, and 1.18%).

hygroscopicity-CCN closure study. Several such closure studies have previously been done on atmospheric aerosols, however, always for shorter time periods [*Kammermann et al.*, 2010b, and references therein]. The hygroscopicity-CCN closure is often done by comparing measured and predicted CCN number concentrations. In Figure 8 we compare monthly median values of HTDMA- and CCNC-derived κ values instead (the calculation of κ values is described in section 3.1). Comparing κ values was chosen for our closure analysis because it amplifies the differences.

[35] The dry diameters of the HTDMA data (shown in Figure 8) were chosen to match the median critical diameters at the CCNC's *SS* as closely as possible. The HTDMA- and CCNC-derived κ hygroscopicity parameters have similar absolute values and show qualitatively the same size dependence of slightly decreasing κ with decreasing diameter, except for the smallest diameter at which κ increases again slightly. Nevertheless, a slightly more pronounced dry diameter dependence could be identified for the CCNC-derived κ values. *Good et al.* [2010] showed that it is not possible to quantify the individual contributions of potential causes (e.g., measurement uncertainty, shortcomings of κ-Köhler theory, surface tension effects) to these differences between the HTDMA- and CCNC-derived κ values. However, these differences are unimportant for CCN predictions from HTDMA and number size distribution data, given the fact that using $\kappa = 0.30$ instead of $\kappa = 0.20$ just introduces an ~11% prediction bias [see section 4.5 below and sensitivity analysis by *Jurányi et al.* [2010]. This means that HTDMA measurements at subsaturated RH can be used to determine the mean κ value required for reliable CCN number concentration predictions from time resolved number size distribution data at a remote site like the JFJ, confirming the results by *Kammermann et al.* [2010a]. In that sense the long-term hygroscopicity-CCN closure can be considered to be successful. However, it should be kept in mind that aerosols at sites that are much closer to source regions may behave differently.

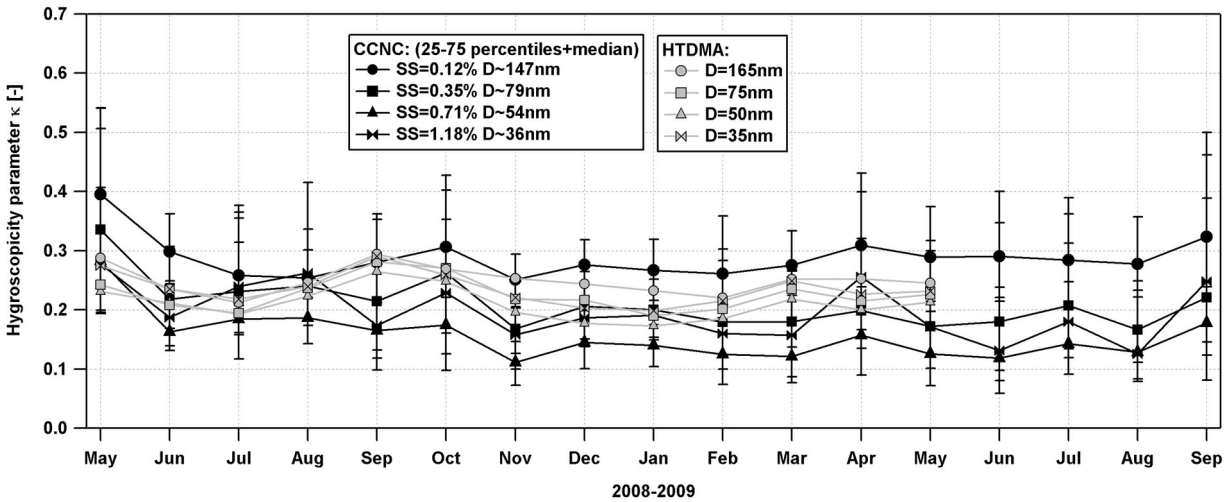

Figure 8. The κ hygroscopicity parameter of the HTDMA (corresponding to the monthly averaged GFs, gray symbols) and of the CCNC (25th, 50th, and 75th percentile of the monthly distributions, black symbols). Different symbols represent the different dry diameters (HTDMA) or the different *SS* (CCNC).

Table 3. Fit Parameters of the Seasonal $N_{CCN}(SS)$ Function[a]

Season	a (cm^{-3})	b ($(cm^3\ \%)^{-1}$)	c
Winter	−2.8	97.8	0.770
Spring	−124.2	413.5	0.3460
Summer	−360.5	812.2	0.259
Autumn	−111.3	323.8	0.3245

[a]See equation (2).

4.5. Calculating CCN Number Concentration From Other Aerosol Properties

[36] Continuous monitoring of atmospheric CCN number concentrations across a wide range of *SS* is only done at a few measurement sites. Furthermore, the primary output of numerical models describing atmospheric aerosols typically provides other aerosol parameters than the CCN number concentration. For this reason we use our comprehensive 17 month data set comprising various aerosol properties to evaluate different methods of varying complexity to infer N_{CCN} from other aerosol parameters. Predictions of N_{CCN} were calculated for every single CCNC data point when both measurements of N_{CCN} and number size distribution were available (94,499 data points at 10 different supersaturations in total).

[37] The simplest method is to assume an *SS*-dependent N_{CCN} which is constant in time. This prediction method completely neglects the temporal variation of the chemical composition as well as of the particle number size distribution (both shape and integrated particle number concentration). The *SS* dependence of N_{CCN} is described with a power law function,

$$N_{CCN}(SS,t) = a + b \cdot SS^c. \quad (2)$$

[38] In order to account for the JFJ-specific strong seasonal cycle of N_{CCN}, the power law function was fitted to the experimental data for each season separately. Resulting fit parameters a, b and c are listed in Table 3 for all four seasons.

[39] The second prediction method is to assume an *SS*-dependent AF, which is constant in time,

$$N_{CCN}(SS,t) = N_{16-570}(t) \cdot \mathrm{AF}(SS). \quad (3)$$

[40] The *SS* dependence of AF was directly obtained from the measurements. The median value of all measured AF values was determined for each investigated *SS*. This was again done for each season separately, in order to account for the distinct seasonal cycle of AF. This method completely neglects the temporal variation of the chemical composition and of the shape of the number size distribution within one season, whereas the temporal variability of the integrated particle number concentration is accounted for by multiplying AF(*SS*) with N_{16-570}. It must be emphasized that

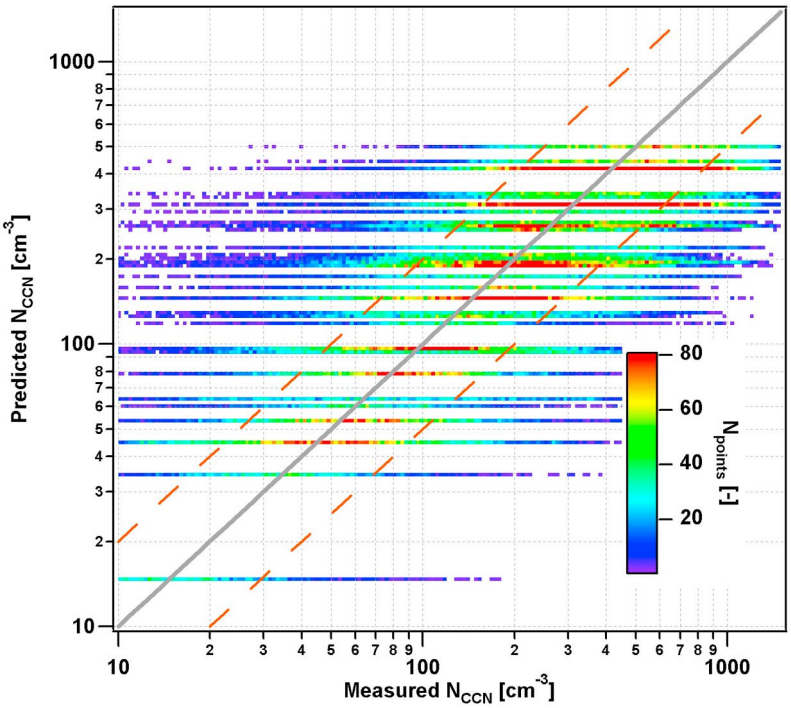

Figure 9. Predicted and measured N_{CCN} during the whole 17 month measurement campaign on a log-log scale with the first, simplest prediction method assuming constant $N_{CCN}(SS)$ for each season. (See text for details.) The color of each pixel represents the number of data points (prediction versus measurement) falling into the area of the pixel (all pixels have equal area on a log-log scale). The gray solid line represents the one-to-one line, and the orange dashed lines correspond to $y = 0.5x$ and $y = 2x$. Note that the seasonally constant $N_{CCN}(SS)$ was chosen such that the overall median prediction equals the overall median measurement.

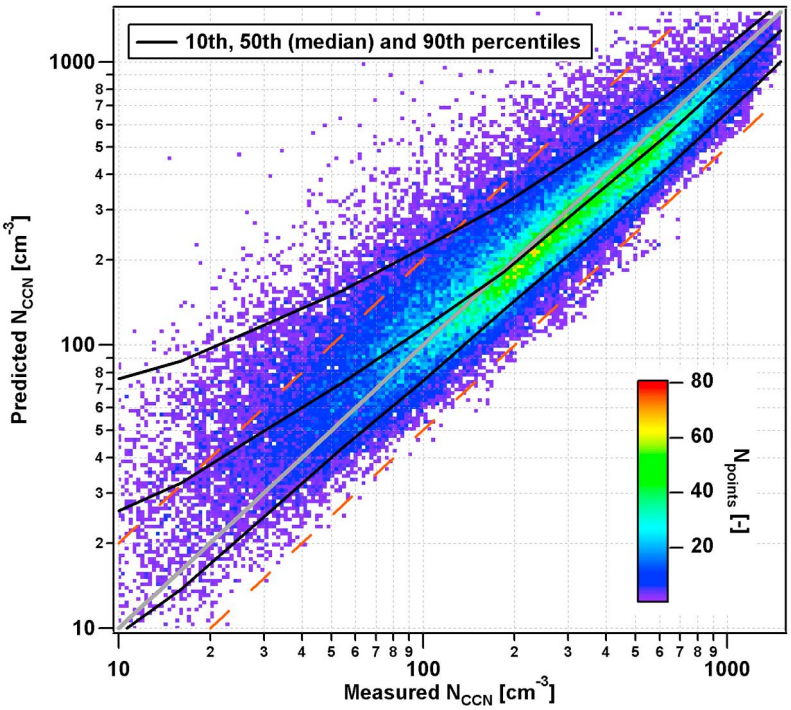

Figure 10. Predicted and measured N_{CCN} during the whole 17 month measurement campaign on a log-log scale with the second prediction method assuming seasonally constant AF(*SS*). (See text for details.) The color of each pixel represents the number of data points (prediction versus measurement) falling into the area of the pixel (all pixels have equal area on a log-log scale). The gray solid line represents the one-to-one line, the orange dashed lines correspond to $y = 0.5x$ and $y = 2x$, and the black lines correspond to the 10th, 50th (median), and 90th percentiles of the distribution of predicted N_{CCN} as a function of measured N_{CCN}. Note that the seasonally constant AF(*SS*) was chosen such that the overall median prediction equals the overall median measurement.

great care has to be taken to use the same lower cutoff diameter for calculating the integrated particle number concentration as well as the AF values.

[41] The third and most sophisticated method of those presented here is to assume a constant time- and size-independent chemical composition, while the temporal variability of the measured particle number size distribution is fully considered. In other words, the mean chemical composition is considered, whereas the temporal variability and size dependence of the composition is ignored. The time and *SS* averaged κ value of 0.20 was chosen to represent the mean composition. This κ value is translated into a time-independent $D_{0,crit}$ for each *SS*, and corresponding $N_{CCN}(SS)$ are obtained by integrating the measured particle number size distributions from $D_{0,crit}(SS)$ to its upper end (570 nm) for every single CCNC data point.

[42] The correlation between measured and predicted N_{CCN} for the whole measurement period and including data from all *SS* is presented in Figures 9, 10 and 11 for the above three prediction methods. Figures 9–11 are not standard correlation plots because of the vast number of individual data points. Raster graphics are shown instead, where the color of each pixel (uniform area on the logarithmic plot) represents the number of data points (prediction versus measurement) falling into the area of the pixel. The gray solid (y = x) and orange dashed lines (y = 0.5x and y = 2x) are to guide the eyes. The black solid lines in Figures 10 and 11 indicate the 10th, 50th (median) and 90th percentiles of the distribution of predicted N_{CCN} as a function of the measured N_{CCN}.

[43] Only 40 different values of predicted N_{CCN} are obtained with the simplest prediction approach (10 different *SS* times 4 seasons), in which $N_{CCN}(SS)$ is to be constant in each season. This explains the horizontal structures of the raster graphic in Figure 9. A considerable fraction of CCN predictions are more than a factor of 2 off the measurement and deviations up to a factor of 10 occur.

[44] The second prediction method performs much better (Figure 10). Most of the predictions are now within a factor of 2 of the measurements. The N_{CCN} predictions are asymmetrically distributed with the maximum data point density below the one-to-one line at any measured N_{CCN}. This is a consequence of the asymmetry of the AF distributions (Figure 5).

[45] The third prediction method has a very good performance (Figure 11), most of the data points from all *SS* fall very close to the one-to-one line across the whole range of measured N_{CCN}. Somewhat increased measurement noise at lower N_{CCN} can most probably be attributed to the limited counting statistics in the particle number size distribution and CCN number concentration measurements.

[46] A more quantitative assessment of the performance of the three different prediction methods is presented in Figure 12, which shows the probability density function

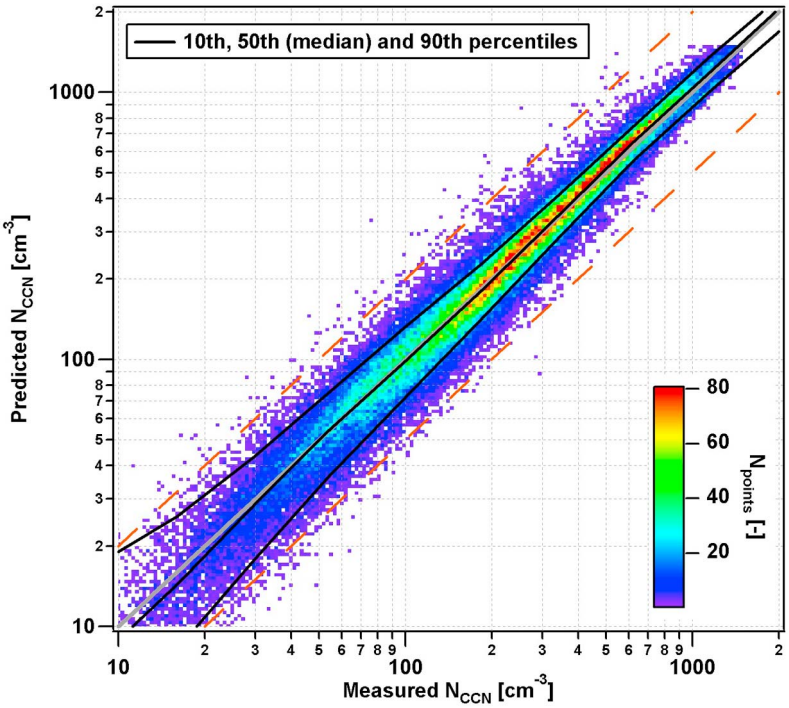

Figure 11. Predicted and measured N_{CCN} during the whole 17 month measurement campaign on a log-log scale with the third prediction method taking time resolved size distribution data into account. (See text for details.) The color of each pixel represents the number of data points (prediction versus measurement) falling into the area of the pixel (all pixels have equal area on a log-log scale). The gray solid line represents the one-to-one line, the orange dashed lines correspond to $y = 0.5x$ and $y = 2x$, and the black lines correspond to the 10th, 50th (median), and 90th percentiles of the distribution of predicted N_{CCN} as a function of measured N_{CCN}. Note that the constant κ value was chosen such that the overall median prediction equals the overall median measurement.

(PDF) of the ratio between predicted and measured N_{CCN} for all data points from all *SS*. Here it is important to emphasize that the chosen constant $N_{CCN}(SS)$, AF(*SS*) and κ required for the first, second and third prediction method, respectively, results in median predicted to measured N_{CCN} ratios of almost unity. The 10th percentiles of the PDFs are 0.36, 0.71 and 0.74 and the 90th percentiles are 2.85, 2.27 and 1.29 for the first, second and third prediction methods, respectively. This means that, for example, for the most sophisticated prediction,80% of the predicted number concentrations fall within 0.74–1.29 times the measured values.

[47] We can conclude from Figures 9–12 that the first, simplest, prediction method should only be used if no better alternative is available. The large prediction errors have to be kept in mind and the propagated errors for any further calculations have to be considered. The second prediction method provides much better results and can be considered as a valid compromise if number size distribution data are not available and a factor of 2 prediction accuracy is sufficient. The third prediction method performs very well and clearly shows that highly time-resolved particle number size distribution data and knowledge about the average chemical composition is enough to reliably predict the instantaneous CCN number concentration at any *SS* with high accuracy. However, one has to be aware that neglecting the temporal variability of the chemical composition at sites that are much closer to the aerosol sources might cause significant prediction bias. *Jurányi et al.* [2010] showed in a chemical composition–CCN closure study at the JFJ that the performance of N_{CCN} predictions cannot be significantly improved by considering the temporal variability of the chemical composition. This can be explained by the limited sensitivity to the chemical composition (see *Jurányi et al.* [2010] for a detailed sensitivity analysis) and the fact that a considerable part of the prediction uncertainty is associated with limited counting statistics in the particle number size distribution data measured at very low particle number concentrations as encountered at the JFJ. The correlation coefficients between predicted and measured N_{CCN} are in the range $r^2 = 0.90–0.94$ for all supersaturations investigated in this study. Achieving this outstanding performance of the N_{CCN} prediction has certainly been facilitated by the relatively slow variability of the remote aerosol at the JFJ. In contrast to that only very few previous CCN closure studies [*Liu et al.*, 1996; *Bougiatioti et al.*, 2009; *Kammermann et al.*, 2010b; *Wang et al.*, 2010] achieved high correlation coefficients $r^2 > 0.8$), even with using time- and sometimes size-resolved chemical composition or hygroscopicity information. Further existing composition-CCN closure studies are discussed by *Jurányi et al.* [2010] and *Kammermann*

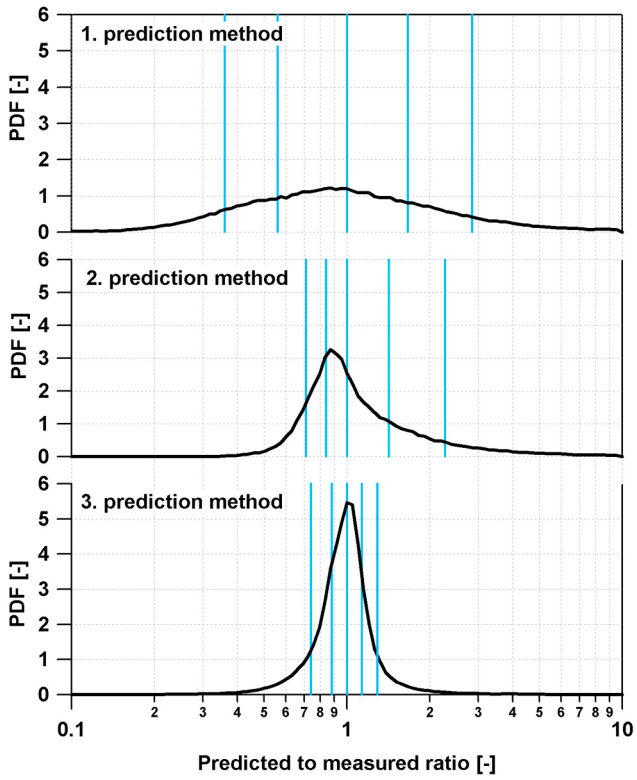

Figure 12. Probability density function (PDF) of the predicted to measured N_{CCN} for the three different prediction methods: method 1, assuming seasonal, time-independent CCN number concentration; method 2, assuming seasonal, time-independent AF; and method 3, taking the full, time-dependent size distribution into account (see text for more details). Blue lines show some percentiles of the distributions (10th, 25th, 50th = median, 75th, and 90th). Note that the constant $N_{CCN}(SS)$, AF(SS) and κ required for the first, second, and third prediction methods, respectively, were chosen such that the median predicted to measured N_{CCN} ratio becomes unity.

et al. [2010b], the latter provides a detailed comparison of hygroscopicity-CCN closure studies.

4.6. Conclusions

[48] For the first time, long-term measurements of N_{CCN} at 10 different supersaturations were shown and analyzed. The measurement site is representative of the free troposphere most of the time, with influence from injections of more polluted PBL air only during the warmer seasons and in the afternoon, as shown here by the diurnal patterns of N_{CCN} and in previous studies. The CCN number concentrations observed at the JFJ are very low even at the highest SS (monthly median values between 113 cm^{-3} and 563 cm^{-3}), such that cloud-droplet activation is likely to occur in the aerosol-limited regime most of the time, in which an increase of particle number concentration due to anthropogenic emissions can be expected to influence the cloud properties. The seasonal pattern of N_{CCN} can be explained by the changes in the total aerosol number concentration and by the shift of the aerosol size distribution toward somewhat bigger sizes in summer. The hygroscopicity of the aerosols remains stable throughout the year which is reflected by the nearly constant monthly critical dry diameter values. Even though there is no seasonal variability in the critical dry diameter, it still exhibits a very slight diurnal variation indicating that the injections from the PBL bring less hygroscopic aerosol to the site (most probably less aged and with a higher fraction of organic compounds).

[49] Different methods with different simplifications were tested to predict N_{CCN} throughout the whole measurement campaign. Assuming a seasonally constant $N_{CCN}(SS)$ results in a poor prediction, with a significant fraction of data points with more than a factor of 2 difference between prediction and measurement. Significantly better prediction performance is obtained if the variability of the total particle concentration is taken into account via using time-resolved total particle number concentration data multiplied by a seasonally constant AF(SS). Excellent accuracy of N_{CCN} predictions was achieved with taking the time-dependent size distribution data and the average chemical composition into account via assuming constant $D_{0,crit}(SS)$. With this method, N_{CCN} could be reliably predicted for the whole measurement period and at any SS. Eighty percent of the predicted N_{CCN} lie between 0.74 and 1.29 times the measured N_{CCN}. It can be expected that this method with the mean $D_{0,crit}(SS)$ values reported in this study also provides reliable N_{CCN} predictions at other European free tropospheric sites, since aerosol hygroscopic properties measured at the JFJ are representative of the free troposphere at least on a regional if not on a continental scale [*Kammermann et al.*, 2010a] and N_{CCN} is relative insensitive to changes in the chemical composition [*Jurányi et al.*, 2010].

Appendix A

[50] Even when both CPC and SMPS measure perfectly accurately, the integrated number concentration, N_{16-570}, is expected to be smaller than the total number concentration of particles, N_{10}, measured by the CPC, because the diameter range covered by the SMPS (16–570 nm) is smaller than the same of the CPC (>10 nm). N_{16-570} and N_{10} should be equal only if there are no aerosol particles with diameters below 16 nm or above 570 nm. In this case any disagreement between N_{16-570} and N_{10} is related to instrumental/measurement errors and can be used to determine a correction factor. The number concentration of the particles above 570 nm at JFJ can be neglected, which was confirmed by the number concentration of particles measured by an optical particle counter (OPC, Grimm Dustmonitor 1.108).

[51] Contrary to this, a substantial number fraction of the aerosol population might be found below 16 nm. In this case, even if the SMPS measures perfectly, there might be a substantial difference between the N_{10} and N_{16-570}. The number ratio of N_{16-30} (particles between 16 and 30 nm) to N_{16-570} was used as a proxy for the presence of the small particles, assuming that if there are only very few particles between 16 and 30 nm, then there won't be many between 10 and 16 nm either. The periods without small particles were then used to determine the correction factor for the SMPS, following the approach detailed by *Jurányi et al.* [2010]. The correction factor (Figure A1) was determined for every day, thereby always considering a time-centered

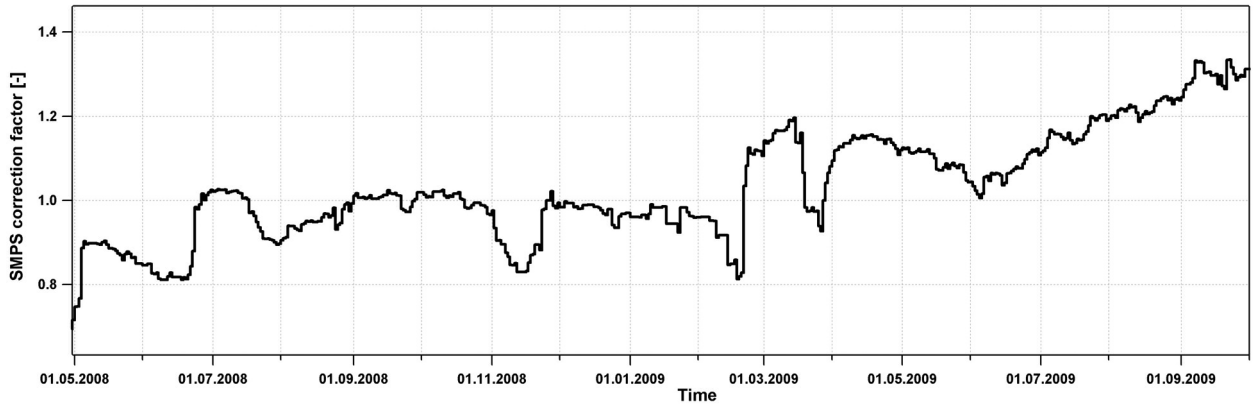

Figure A1. The SMPS correction factor as a function of time.

window of 21 days. The size-independent SMPS correction was then done by dividing the measured number size distributions with the resulting time-dependent correction factor.

[52] The reason for the disagreement between the SMPS and the CPC has been identified to be small leaks at the connectors of the membrane pump in the sheath/excess air loop. Consequences for a system operated with a closed-loop sheath/excess air flow setup and a 10:1 flow ratio are as follows: A small decrease of the sheath air flow rate by 3% due to leakage results in a 30% decrease of the polydisperse sample flow rate, if the excess air flow rate and the monodisperse sample flow pulled by the CPC remain stable. The effects of such a small flow rate alteration are as much as a ~17% percent increase of the transfer function area ("detection efficiency") independent of particle diameter, while the sizing bias remains smaller than 1.1% across the whole diameter range, which is within typical sizing accuracy. Effects of a similar alteration of the excess flow rate are equivalent. For this reason it is justified to apply a size-independent constant correction factor to the number size distribution data.

[53] **Acknowledgments.** We thank the International Foundation High Altitude Research Stations Jungfraujoch and Gornergrat (HFSJG) for the opportunity to perform experiments on the Jungfraujoch. We would like to thank S. F. Seiler and J. M. Fischer for taking care of our instrumentation and us at the Jungfraujoch. Financial support from MeteoSwiss in the framework of the Global Atmosphere Watch program, from the Swiss National Science Foundation, and from the EU FP6 projects EUCAARI and EUSAAR is gratefully acknowledged.

References

Abbatt, J. P. D., K. Broekhuizen, and P. P. Kumal (2005), Cloud condensation nucleus activity of internally mixed ammonium sulfate/organic acid aerosol particles, *Atmos. Environ.*, *39*(26), 4767–4778.

Andreae, M. O., and D. Rosenfeld (2008), Aerosol-cloud-precipitation interactions. Part 1. The nature and sources of cloud-active aerosols. *Earth Sci. Rev.*, *89*(1–2), 13–41.

Baltensperger, U., H. W. Gäggeler, D. T. Jost, M. Lugauer, M. Schwikowski, E. Weingartner, and P. Seibert (1997), Aerosol climatology at the high-alpine site Jungfraujoch, Switzerland, *J. Geophys. Res.*, *102*(D16), 19,707–19,715, doi:10.1029/97JD00928.

Baltensperger, U., M. Schwikowski, D. T. Jost, S. Nyeki, H. W. Gäggeler, and O. Poulida (1998), Scavenging of atmospheric constituents in mixed phase clouds at the high-alpine site Jungfraujoch. Part I: Basic concept and aerosol scavenging by clouds, *Atmos. Environ.*, *32*(23), 3975–3983.

Bougiatioti, A., C. Fountoukis, N. Kalivitis, S. N. Pandis, A. Nenes, and N. Mihalopoulos (2009), Cloud condensation nuclei measurements in the marine boundary layer of the Eastern Mediterranean: CCN closure and droplet growth kinetics, *Atmos. Chem. Phys.*, *9*(18), 7053–7066.

Broekhuizen, K., R. Y. W. Chang, W. R. Leaitch, S. M. Li, and J. P. D. Abbatt (2006), Closure between measured and modeled cloud condensation nuclei (CCN) using size-resolved aerosol compositions in downtown Toronto, *Atmos. Chem. Phys.*, *6*(9), 2513–2524.

Chang, R. Y.-W., P. S. K. Liu, W. R. Leaitch, and J. P. D. Abbatt (2007), Comparison between measured and predicted CCN concentrations at Egbert, Ontario: Focus on the organic aerosol fraction at a semi-rural site, *Atmos. Environ.*, *41*(37), 8172–8182.

Collaud Coen, M., E. Weingartner, S. Nyeki, J. Cozic, S. Henning, B. Verheggen, R. Gehrig, and U. Baltensperger (2007), Long-term trend analysis of aerosol variables at the high-alpine site Jungfraujoch, *J. Geophys. Res.*, *112*, D13213, doi:10.1029/2006JD007995.

Collaud Coen, M., E. Weingartner, M. Furger, S. Nyeki, A. S. H. Prévôt, M. Steinbacher, and U. Baltensperger (2011), Planetary boundary influence at the Jungfraujoch analyzed by aerosol cycles and synoptic weather types, *Atmos. Chem. Phys. Discuss.*, *11*, 985–1024.

Cruz, C. N., and S. N. Pandis (1997), A study of the ability of pure secondary organic aerosol to act as cloud condensation nuclei, *Atmos. Environ.*, *31*(15), 2205–2214.

Dusek, U., et al. (2006), Size matters more than chemistry for cloud-nucleating ability of aerosol particles, *Science*, *312*(5778), 1375–1378.

Gerber, H. E., W. A. Hoppel, and T. A. Wojciechowski (1997), Experimental-verification of theoretical relationship between size and critical supersaturation of salt nuclei, *J. Atmos. Sci.*, *34*(11), 1836–1841.

Good, N., et al. (2010), Widening the gap between measurement and modelling of secondary organic aerosol properties?, *Atmos. Chem. Phys.*, *10*(6), 2577–2593.

Gunthe, S. S., et al. (2009), Cloud condensation nuclei in pristine tropical rainforest air of Amazonia: Size-resolved measurements and modeling of atmospheric aerosol composition and CCN activity, *Atmos. Chem. Phys.*, *9*(19), 7551–7575.

Henning, S., E. Weingartner, S. Schmidt, M. Wendisch, H. W. Gäggeler, and U. Baltensperger (2002), Size-dependent aerosol activation at the high-alpine site Jungfraujoch (3580 m asl), *Tellus, Ser. B*, *54*(1), 82–95.

Intergovernmental Panel on Climate Change (IPCC) (2007), *Climate Change 2007: The Physical Science Basis. Contribution of Working Group I to the Fourth Assessment Report of the Intergovernmental Panel on Climate Change*, Cambridge Univ. Press, Cambridge, U. K.

Jurányi, Z., M. Gysel, E. Weingartner, P. F. DeCarlo, L. Kammermann, and U. Baltensperger (2010), Measured and modelled cloud condensation nuclei concentration at the high alpine site Jungfraujoch, *Atmos. Chem. Phys.*, *10*(22), 7891–7906.

Kammermann, L., M. Gysel, E. Weingartner, and U. Baltensperger (2010a), 13-month climatology of the aerosol hygroscopicity at the free tropospheric site Jungfraujoch (3580 m a.s.l.), *Atmos. Chem. Phys.*, *10*(22), 10,717–10,732.

Kammermann, L., M. Gysel, E. Weingartner, H. Herich, D. J. Cziczo, T. Holst, B. Svenningsson, A. Arneth, and U. Baltensperger (2010b), Subarctic atmospheric aerosol composition: 3. Measured and modeled properties of cloud condensation nuclei (CCN), *J. Geophys. Res.*, *115*, D04202, doi:10.1029/2009JD012447.

Köhler, H. (1936), The nucleus in and the growth of hygroscopic droplets, *Trans. Faraday Soc.*, *32*(2), 1152–1161.

Lance, S., et al. (2009), Cloud condensation nuclei activity, closure, and droplet growth kinetics of Houston aerosol during the Gulf of Mexico Atmospheric Composition and Climate Study (GoMACCS), *J. Geophys. Res.*, *114*, D00F15, doi:10.1029/2008JD011699.

Liu, P. S. K., W. R. Leaitch, C. M. Banic, S. M. Li, D. Ngo, and W. J. Megaw (1996), Aerosol observations at Chebogue Point during the 1993 North Atlantic Regional Experiment: Relationships among cloud condensation nuclei, size distribution, and chemistry, *J. Geophys. Res.*, *101*(D22), 28,971–28,990, doi:10.1029/96JD00445.

Lohmann, U., and J. Feichter (2005), Global indirect aerosol effects: A review, *Atmos. Chem. Phys.*, *5*(3), 715–737.

Lugauer, M., U. Baltensperger, M. Furger, H. W. Gäggeler, D. T. Jost, M. Schwikowski, and H. Wanner (1998), Aerosol transport to the high Alpine sites Jungfraujoch (3454 m asl) and Colle Gnifetti (4452 m asl), *Tellus, Ser. B*, *50*(1), 76–92.

McFiggans, G., et al. (2006), The effect of physical and chemical aerosol properties on warm cloud droplet activation, *Atmos. Chem. Phys.*, *6*(9), 2593–2649.

Medina, J., A. Nenes, R. Sotiropoulou, and L. Cottrell (2007), Cloud condensation nuclei closure during the International Consortium for Atmospheric Research on Transport and Transformation 2004 campaign: Effects of size-resolved composition, *J. Geophys. Res.*, *112*, D10S31, doi:10.1029/2006JD007588.

Nessler, R., N. Bukowiecki, S. Henning, E. Weingartner, B. Calpini, and U. Baltensperger (2003), Simultaneous dry and ambient measurements of aerosol size distributions at the Jungfraujoch, *Tellus, Ser. B*, *55*(3), 808–819.

Nyeki, S., F. Li, E. Weingartner, N. Streit, I. Colbeck, H. W. Gäggeler, and U. Baltensperger (1998), The background aerosol size distribution in the free troposphere: An analysis of the annual cycle at a high-alpine site, *J. Geophys. Res.*, *103*(D24), 31,749–31,761, doi:10.1029/1998JD200029.

Nyeki, S., et al. (2000), Convective boundary layer evolution to 4 km asl over high-alpine terrain: Airborne lidar observations in the Alps, *Geophys. Res. Lett.*, *27*(5), 689–692, doi:10.1029/1999GL010928.

Petters, M. D., and S. M. Kreidenweis (2007), A single parameter representation of hygroscopic growth and cloud condensation nucleus activity, *Atmos. Chem. Phys.*, *7*(8), 1961–1971.

Pringle, K. J., H. Tost, A. Pozzer, U. Pöschl, and J. Lelieveld (2010), Global distribution of the effective aerosol hygroscopicity parameter for CCN activation, *Atmos. Chem. Phys.*, *10*(12), 5241–5255.

Raymond, T. M., and S. N. Pandis (2003), Formation of cloud droplets by multicomponent organic particles, *J. Geophys. Res.*, *108*(D15), 4469, doi:10.1029/2003JD003503.

Reutter, R., H. Su, J. Trentmann, M. Simmel, D. Rose, S. S. Gunthe, H. Wernli, M. O. Andreae, and U. Pöschl (2009), Aerosol- and updraft-limited regimes of cloud droplet formation: Influence of particle number, size and hygroscopicity on the activation of cloud condensation nuclei (CCN), *Atmos. Chem. Phys.*, *9*(18), 7067–7080.

Roberts, G. C., and A. Nenes (2005), A continuous-flow streamwise thermal-gradient CCN chamber for atmospheric measurements, *Aerosol Sci. Technol.*, *39*(3), 206–221.

Rose, D., S. S. Gunthe, E. Mikhailov, G. P. Frank, U. Dusek, M. O. Andreae, and U. Pöschl (2008), Calibration and measurement uncertainties of a continuous-flow cloud condensation nuclei counter (DMT–CCNC): CCN activation of ammonium sulfate and sodium chloride aerosol particles in theory and experiment, *Atmos. Chem. Phys.*, *8*(5), 1153–1179.

Rose, D., A. Nowak, P. Achtert, A. Wiedensohler, M. Hu, M. Shao, Y. Zhang, M. O. Andreae, and U. Pöschl (2010), Cloud condensation nuclei in polluted air and biomass burning smoke near the mega-city Guangzhou, China. Part 1: Size-resolved measurements and implications for the modeling of aerosol particle hygroscopicity and CCN activity, *Atmos. Chem. Phys.*, *10*(7), 3365–3383.

Rosenfeld, D., U. Lohmann, G. B. Raga, C. D. O'Dowd, M. Kulmala, S. Fuzzi, A. Reissell, and M. O. Andreae (2008), Flood or drought: How do aerosols affect precipitation?, *Science*, *321*(5894), 1309–1313.

Schüepp, M. (1979), *Klimatologie der Schweiz*, band III, *Witterungsklimatologie*, Schweiz. Meteorol. Anstalt, Zurich, Switzerland.

Sihto, S.-L., et al. (2010), Seasonal variation of CCN concentrations and aerosol activation properties in boreal forest, *Atmos. Chem. Phys. Discuss.*, *10*, 28,231–28,272.

Sjogren, S., M. Gysel, E. Weingartner, M. R. Alfarra, J. Cozic, J. Crosier, H. Coe, and U. Baltensperger (2008), Hygroscopicity of the submicrometer aerosol at the high-alpine site Jungfraujoch, 3580 m a.s.l., Switzerland, *Atmos. Chem. Phys.*, *8*(18), 5715–5729.

Su, H., D. Rose, Y. F. Cheng, S. S. Gunthe, A. Massling, M. Stock, A. Wiedensohler, M. O. Andreae, and U. Pöschl (2010), Technical note: Hygroscopicity distribution concept for measurement data analysis and modeling of aerosol particle hygroscopicity and CCN activity, *Atmos. Chem. Phys.*, *10*(15), 7489–7503.

Swietlicki, E., et al. (2008), Hygroscopic properties of submicrometer atmospheric aerosol particles measured with H-TDMA instruments in various environments—A review, *Tellus, Ser. B*, *60*(3), 432–469.

Topping, D. O., G. B. McFiggans, and H. Coe (2005), A curved multi-component aerosol hygroscopicity model framework: Part 1. Inorganic compounds, *Atmos. Chem. Phys.*, *5*(5), 1205–1222.

Wang, J., M. J. Cubison, A. C. Aiken, J. L. Jimenez, and D. R. Collins (2010), The importance of aerosol mixing state and size-resolved composition on CCN concentration and the variation of the importance with atmospheric aging of aerosols, *Atmos. Chem. Phys.*, *10*(15), 7267–7283.

Weingartner, E., S. Nyeki, and U. Baltensperger (1999), Seasonal and diurnal variation of aerosol size distributions ($10 < D < 750$ nm) at a high-alpine site (Jungfraujoch 3580 m asl), *J. Geophys. Res.*, *104*(D21), 26,809–26,820.

U. Baltensperger, N. Bukowiecki, M. Gysel, Z. Jurányi, L. Kammermann, and E. Weingartner, Laboratory of Atmospheric Chemistry, Paul Scherrer Institut, CH-5232 Villigen, Switzerland. (martin.gysel@psi.ch)